Using AVIRIS Data to Map and Characterize Subaerially and Subaqueously Erupted BasalticVolcanic Tephras: The Challenge of Mapping Low-Albedo Materials

William H. Farrand[1]

1.0   Introduction

Increases in the signal-to-noise ratio (SNR) in AVIRIS has enabled the mapping and characterization of low albedo materials. Low albedo materials of interest include certain soils, man-made materials (asphalt, certain building materials, tires, etc.), and basaltic lava flows and ashes. Early in its history, the response of the AVIRIS sensor was not sensitive enough so that these low albedo materials could be reliably mapped. However, as indicated by Green and Pavri (2002) the noise equivalent delta radiance (NEdL) of AVIRIS in the 2001 flight season was below 0.010 in all but the shortest wavelength channels. This is approximately a ten-fold improvement from the 1989 flight season when NEdL was closer to 0.1 (Green et al., 1990). In the current investigation, AVIRIS data from the 2002 flight season collected over the Pavant Butte tuff cone, Tabernacle Hill tuff ring, and an associated lava flow in the Black Rock Desert of west central Utah were examined to determine how well these generally low albedo volcanic lavas and tephras could be discriminated from background materials. The Pavant Butte tuff cone was examined by the author in an earlier study with a 1989 AVIRIS dataset (Farrand and Singer, 1991).

2.0   Field Area

Figure 1 shows the location of the Pavant Butte area and the outline of the portion of the AVIRIS flightline that was examined. Tabernacle Hill and Pavant Butte are examples of, respectively, a tuff ring and a tuff cone. Such landforms are part of a continuum of volcanic landforms that are produced when magmas erupt in the presence of water. They represent different amounts of water present at the vent at the time of eruption. Tuff cones are produced from high water/magma ratios representative of eruption into standing water and tuff rings result from a lower water/magma ratio (Wohletz and Sheridan, 1983). Pavant Butte was erupted into Pleistocene Lake Bonneville in west-central Utah between 16,000 and 15,300 years ago (Oviatt and Nash, 1989). It consists of a partial cone that is composed of massively bedded ashes which are highly palagonitized and cemented into tuff. These palagonite tuff beds lie atop fresh to poorly palagonitized ash and tuff beds. The ash beds lie atop lacustrine sediments. Ash and cinders from the Pavant Butte eruption are prominent as a component of the soils surrounding the tuff cones. The AVIRIS scene analyzed in this study also contains a number of ephemeral lakes or playas some of which were apparently wet at the time of the overflight. South of Pavant Butte lies the younger, moderately palagonitized Tabernacle Hill tuff ring. Tabernacle Hill lies atop a weathered basalt flow. The age of the Tabernacle Hill eruptions is between 14,500 and 14,300 years ago (Oviatt and Nash, 1989). Between Pavant Butte and Tabernacle Hill lies a more recent, relatively fresh, low albedo basalt flow.

[1] Farr View Consulting, Thornton, Colorado and Space Science Institute, Boulder, Colorado, E-mail: farrand@ricochet.com
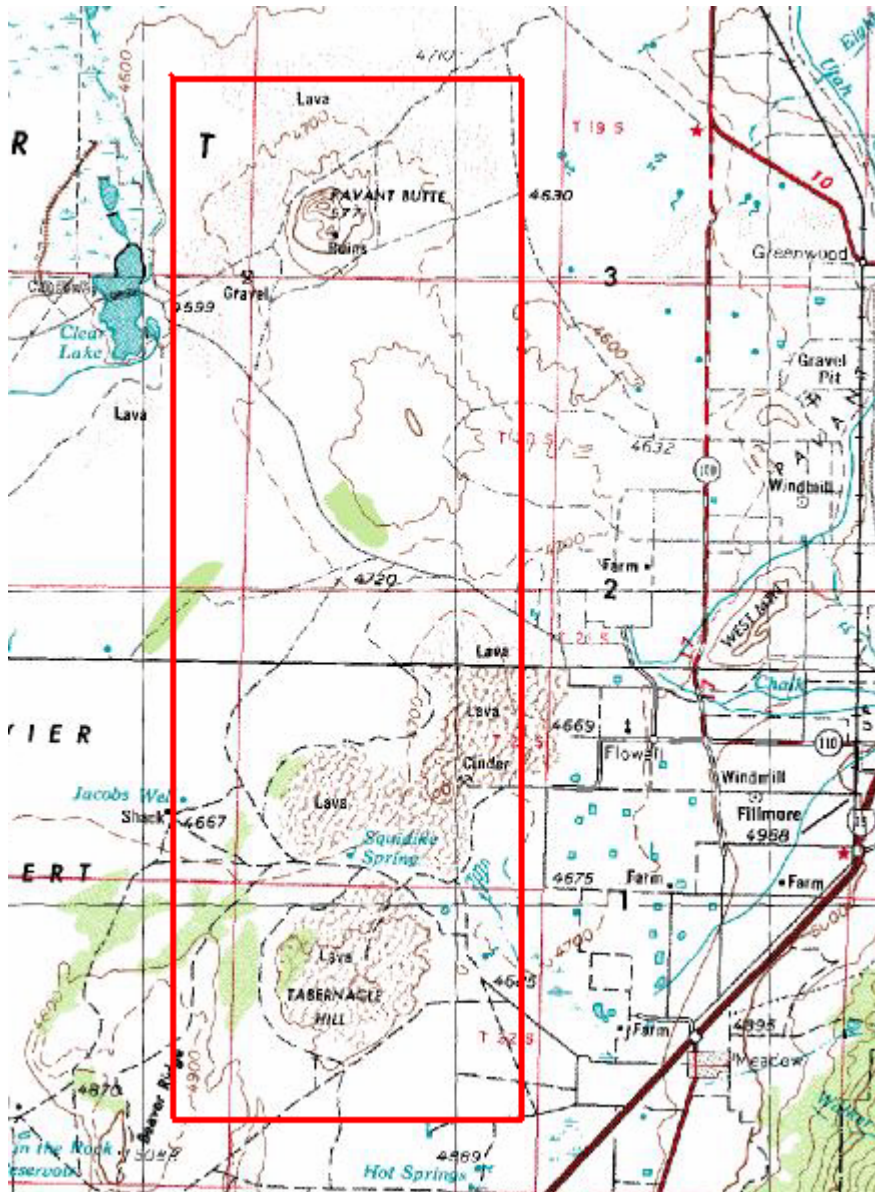
Figure 1. Portion of topographic map of the Pavant Butte area. The subsection of the AVIRIS flightline discussed here is outlined.

3.0   Materials of Interest

Reflectance spectra of hydrovolcanic tephras from Pavant Butte and the fresh basalt flow, extracted from the AVIRIS scene, are presented in Figure 2. The reflectance of the Tabernacle hill tuffs is approximately the same as that of the poorly palagonitized tuff shown in Figure 2. The well palagonitized tuff is distinguished by a distinct Fe^{3+} crystal field band just shortwards of 1 μm, deep water absorption features, and a small sheet silicate vibrational overtone at 2.3 μm. In the poorly palagonitized material, the "1 μm" feature is caused by both Fe^{3+} in the palagonite and Fe^{2+} in the unpalagonitized glass. Water absorption features are weak to absent. The highly palagonitized tuff is relatively bright while the poorly palagonitized tuff is characterized by relatively low reflectance values, on the order of 20%. The relatively unaltered ash has reflectance values below 10%. More detail on the spectroscopic characteristics of Pavant Butte tephras is provided in Farrand and Singer (1992).
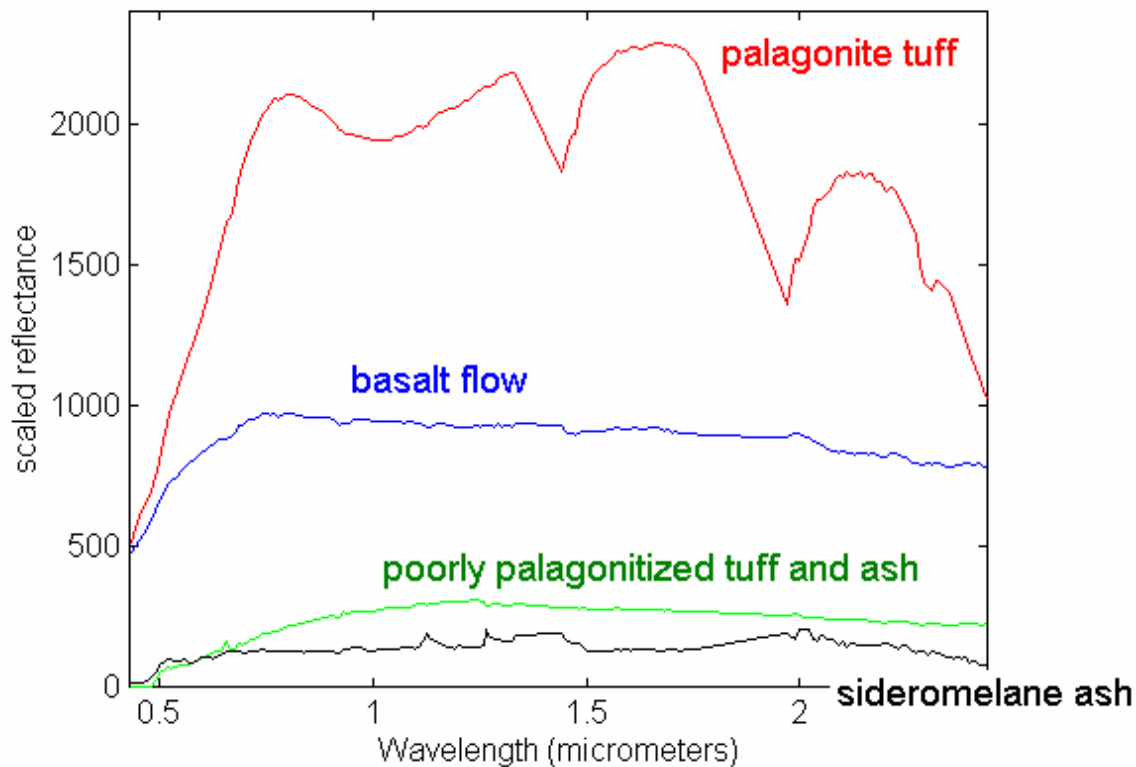
Figure 2. Reflectance spectra of hydrovolcanic tephras from Pavant Butte and fresh basalt flow as extracted from the AVIRIS data. Spectra have been scaled by a factor of 5000. Note that even the low reflectance sideromelane (basaltic glass) ash has discernable spectral shape.

The surrounding lacustrine sediments include several clay minerals as well as the evaporite mineral gypsum. There are aeolian sediments which to the naked eye appear reddish and whose reflectance spectra indicate the presence of iron and a weak 2.2 mm band indicative of a dioctahedral clay phase. The recent basaltic lava flow in the central part of the scene has low reflectance values. In addition to the volcanic materials and aeolian and lacustrine sediments, some circularly irrigated agricultural fields are also present in the scence near Tabernacle Hill and the recent lava flow.

4.0   Data
The hyperspectral data examined here were collected on October 8, 2002 by NASA's Airborne Visible/Infrared Imaging Spectrometer (AVIRIS). The data, as supplied by the AVIRIS data lab, were provided in a geometrically corrected format (Boardman, 1999). In order to eliminate null pixels at the borders of the scene that were introduced by the geometric correction, the data were spatially subsampled to a 688 by 2048 subsection. It is this spatial coverage that is outlined in Figure 1 and shown in the color composites of Figure 4. The data were corrected to surface reflectance by means of the HATCH atmospheric correction software (Qu et al., 2000). Spectral "polishing" of the data was achieved through application of the EFFORT software (Boardman, 1998) resident in ENVI.

5.0   Results

Selection of an initial set of image endmembers was achieved by applying the "standard" ENVI processing steps of Minimum Noise Fraction (MNF) transformation, Pixel Purity Index pixel selection, and n-Dimensional visualization (RSI, 2002). This initial set of image endmembers was used as input to the linear spectral mixture analysis (SMA) routine contained in ENVI. SMA was run iteratively in order to obtain additional endmembers indicated in the root mean square (RMS) error image (Adams et al., 1993). The final set of image endmember spectra is shown in Figure 3. The endmember materials include the highly palagonitized tuff of Pavant Butte, vegetation, oxidized cinders associated with the fresh basalt flow and several playa endmembers. A surface class that is notably absent from this set of endmembers is the basalt flow itself. The flow is one of the most obvious components of the scene upon visual inspection of a simple color composite (such as Figure 4a).   However, it is a low albedo material and in running SMA on standard reflectance or radiance data, materials which are higher in albedo will be preferentially selected as required image endmembers.

In order to remove the effects of albedo, a hyperspherical directional cosine (HSDC) transformation (Pouch and Campagna, 1990) was applied to the data. Color composites of HSDC transformed data produced color contrasts much more vivid than composites of the non-transformed data. In Figure 4, a three band color composite of the original AVIRIS data is shown along with a composite of the same bands of the HSDC transformed data. In the color composite of the HSDC transformed data, low albedo materials such as the basalt flow and
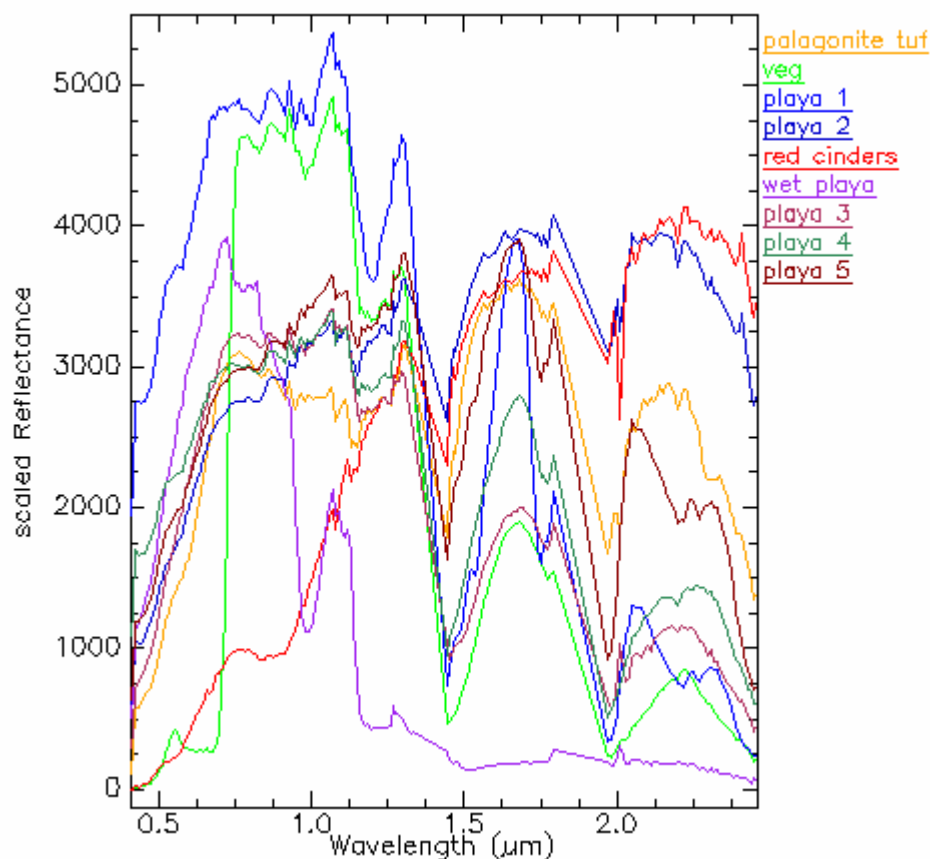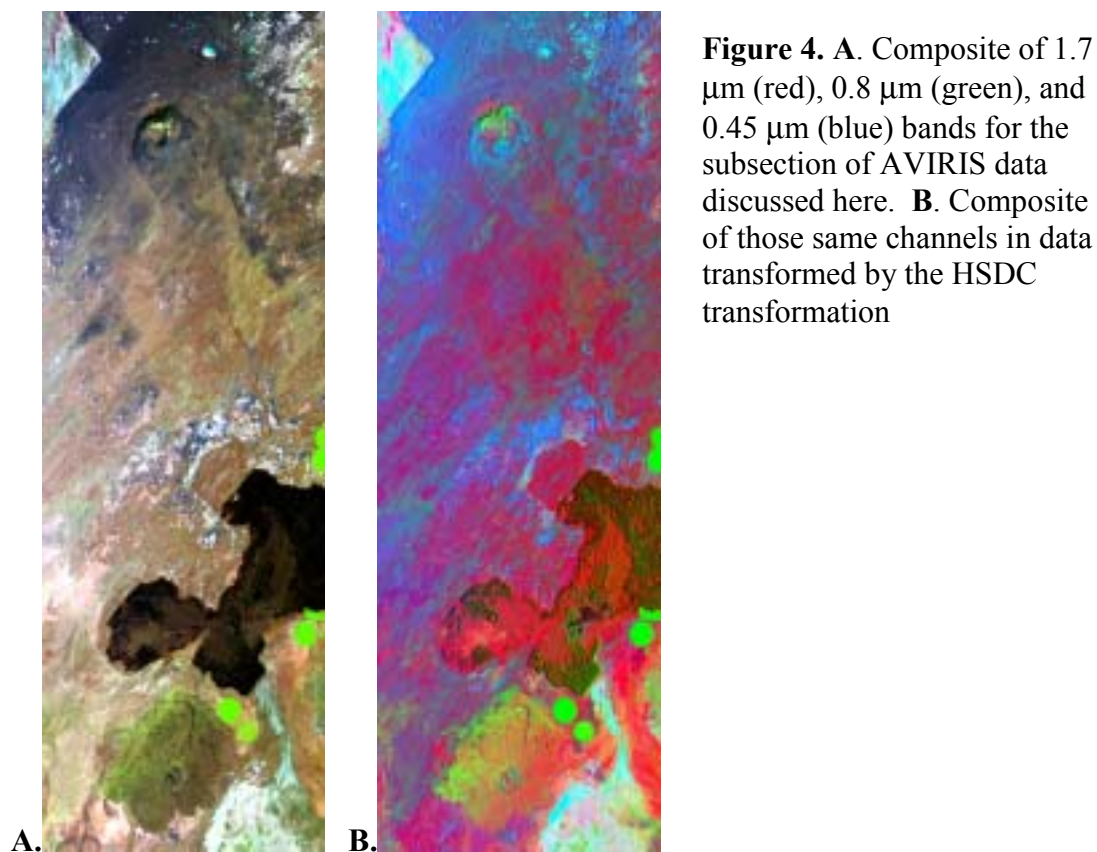

Figure 3. Image endmember spectra derived from iterative spectral mixture analysis of non-albedo normalized AVIRIS data for the Pavant Butte area.

Figure 4. A. Composite of 1.7 μm (red), 0.8 μm (green), and 0.45 μm (blue) bands for the subsection of AVIRIS data discussed here. **B**. Composite of those same channels in data transformed by the HSDC transformation

exposures of the unaltered Pavant Butte ash show up as red. Iterative SMA was applied to the HSDC-transformed data and an endmember required by this analysis was the basalt flow. The resulting fraction image of the basalt endmember also displays higher contrast against the background than when the same pixels are averaged to produce a comparable image endmember set and run against the original/non-albedo normalized data (Figure 5).

Application of the HSDC transformation also helped to improve the mapping of the low albedo ashes associated with Pavant Butte and Tabernacle Hill. Fraction images of the relative abundance of the highly palagonitized tuff and the poorly palagonitized tephras associated with Pavant Butte and Tabernacle Hill were produced via application of constrained energy minimization (CEM) (Farrand and Harsanyi, 1997) and foreground / background analysis (FBA) (Smith et al., 1994). The highest fractions (fractions greater than 0.4) from these fraction images were thresholded and these results are presented in Figure 6. While the ability to map out the highly palagonitized tuff of Pavant Butte was demonstrated in a previous study with relatively low SNR 1989 AVIRIS data (Farrand and Singer, 1991), the lower albedo tephras could not be uniquely mapped out with that data set and the ability to do so in this study is attributed to the increase in instrumental SNR.
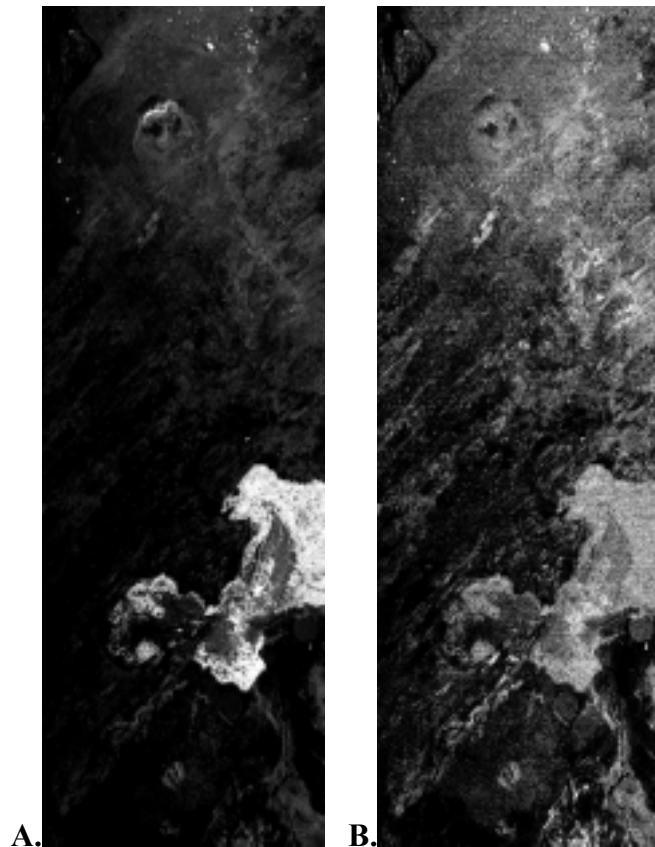
Figure 5. A. Fraction image for basalt flow image endmember as derived and run against the HSDC transformed data. **B**. Basalt fraction image as derived and run against non-albedo normalized data.

A.   B.

While the influence of albedo on SMA is profound, it should be noted that other processing techniques can be more insensitive to the effects of albedo. A spectral feature fitting approach such as is implemented in ENVI and which is a critical component of the USGS Tetracorder (Clark et al., 2003) software requires that the data have the continuum removed. Such a continuum removal is a *de facto* albedo normalization. The Spectral Angle Mapper technique (Kruse et al., 1993) is also insensitive to albedo differences.

6.0   Conclusions

The ability to map low albedo materials in AVIRIS data was demonstrated in this study. The materials of interest in this investigation were volcanic lava flows and tephras of the Black Rock Desert of west central Utah. It was demonstrated that image endmember spectra selected by iterative SMA are skewed towards high albedo materials. Hence, even a major low albedo component in the scene, such as the basalt flow in the Pavant Butte scene, that is readily apparent to the observer in color composites is not a required endmember in iterative SMA of non-albedo normalized data. Forcing the issue, and including such a low albedo endmember in SMA of the non-albedo normalized data, results in a fraction image in which there is low contrast between the target endmember and the background (Figure 5). A better representation of what materials in the scene are truly spectrally unique is obtained by conducting iterative SMA on albedo normalized data. In this study, the HSDC transformation (Pouch and Campagna, 1990) was used to remove albedo differences. Running SMA, or a related technique such as FBA, on the albedo normalized data also serves to increase the contrast between target and background in the the resulting fraction image.

By using the high SNR 2002 AVIRIS data and the HSDC transformation, it was demonstrated that even the low albedo, relatively spectrally featureless poorly palagonitized tephras associated with tuff rings and portions of tuff cones could be uniquely mapped. These materials could not be uniquely identified in an earlier study that was conducted using 1989 flight season AVIRIS data (Farrand and Singer, 1991).
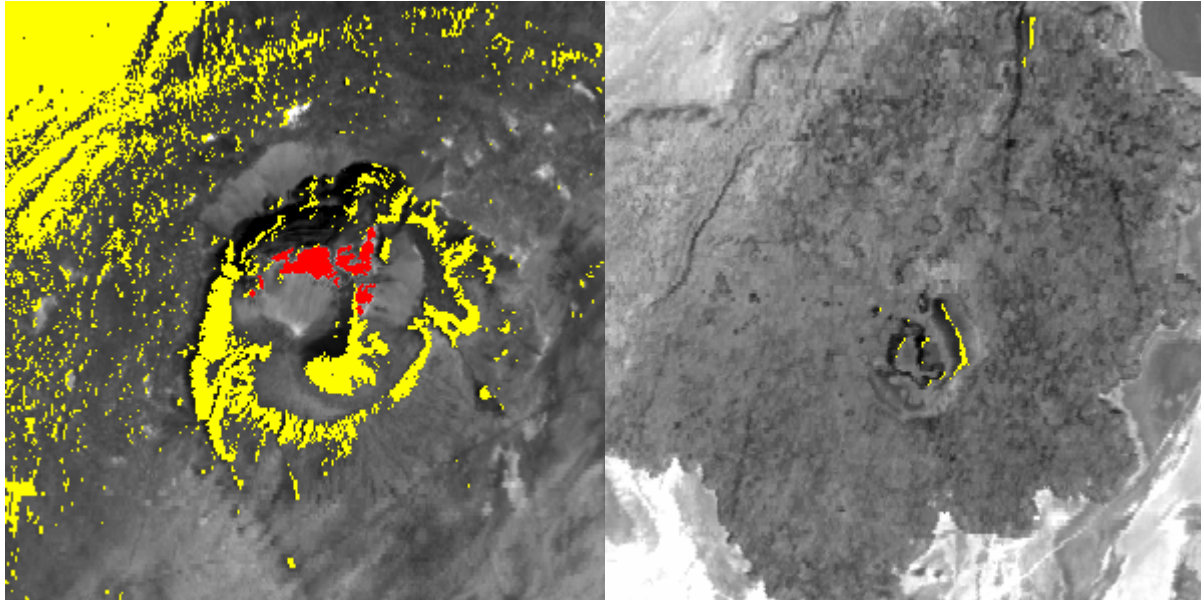

Figure 6. 1.7 μm band with overlay of highest (> 0.4) fractions of highly palagonitized tuff (red) and poorly palagonitized tuff and ash (yellow) over Pavant Butte (left) and Tabernacle Hill (right). Note the absence of highly palagonitized tuff at Tabernacle Hill.

7.0 Acknowledgements

8.0 References

Adams, J.B., M.O. Smith, and A.R. Gillespie, 1993, Imaging spectroscopy: Interpretation based on spectral mixture analysis. In *Remote Geochemical Analysis: Elemental and Mineralogical Composition*, edited by C.M. Pieters and P.A.J. Englert (New York: Cambridge University Press), pp. 145-166.

Boardman, J.W., 1999, Precision geocoding of low altitude AVIRIS data: Lessons learned in 1998. *Proc. 8th JPL Airborne Earth Science Workshop*, (R.O. Green, Ed.), JPL Pub. 99-17, Jet Propulsion Laboratory, Pasadena, California, pp.63-68.

Boardman, J.W., 1998, Post-ATREM polishing of AVIRIS apparent reflectance data using EFFORT: A lesson in accuracy versus precision. *Proc. 7th JPL Airborne Earth Science Workshop*, (R.O. Green, ed.), JPL Publication 97-21, Vol. 1, Jet Propulsion Laboratory, Pasadena, California, pp 53.

Clark, R.N. et al. (7 others), 2003, Imaging spectroscopy: Earth and planetary remote sensing with the USGS Tetracorder and expert systems. *J. Geophys. Res.* (in press), http://speclab.cr.usgs.gov/PAPERS/tetracorder.

Farrand, W.H. and J.C. Harsanyi, 1997, Mapping the distribution of mine tailings in the Coeur d'Alene River Valley, Idaho through the use of a Constrained Energy Minimization technique. *Rem. Sens. of Env.* **59**, 64-76.

Farrand, W.H. and R.B. Singer, 1992, Alteration of hydrovolcanic basaltic ash: Observations with visible and near-infrared spectrometry. *J. Geophys. Res.* **97**, 17,393-17,408.

Farrand, W.H. and R.B. Singer, 1991, Spectral analysis and mapping of palagonite tuffs of Pavant Butte, Millard County, Utah. *Geophys. Res. Letters* **18**, 2237-2240.

Green, R.O. and B. Pavri, 2002, AVIRIS in-flight calibration experiment results for 2001, *Proc. 11th JPL Airborne Earth Science Workshop*, (R.O. Green, Ed.), JPL Pub. 03-4, Jet Propulsion Laboratory, Pasadena, California, pp. 125-137.

Green, R.O., J.E. Conel, V. Carrere, C.J. Bruegge, J.S. Margolis, M. Rast, and G. Hoover, 1990, Determination of the in-flight spectral and radiometric characteristics of AVIRIS, *Proc. Second Airborne Visible/Infrared Imaging Spectrometer (AVIRIS) Workshop*, (R.O. Green, Ed.), JPL Pub. 90-54, Jet Propulsion Laboratory, Pasadena, California, pp. 15-34.

Kruse, F.A., A.B. Lefkoff, J.W. Boardman, K.B. Heidebrecht, A.T. Shapiro, P.J. Barloon, and A.F.H. Goetz, 1993, The Spectral Image Processing System (SIPS)- Interactive visualization and analysis of imaging spectrometer data. *Remote Sens. Env.*, **44**, 145-164.

Oviatt, C.G. and W.P. Nash, 1989, Late Pleistocene basaltic ash and volcanic eruptions in the Bonneville basin, *Utah. Geol. Soc. America Bull.*, **101**, 292-303.

Pouch, G.W. and D.J. Campagna, 1990, Hyperspherical direction cosine transformation for separation of spectral and illumination information in digital scanner data. *Photogram. Eng. And Remote Sens.*, **56**, 475-479.

Qu, Z. A.F.H. Goetz, and K.B. Heidebrecht, 2000, High-accuracy atmosphere correction for hyperspectral data (HATCH), *Proc. 9th JPL Airborne Earth Science Workshop*, (R.O. Green, Ed.), JPL Pub. 00-18, Jet Propulsion Laboratory, Pasadena, California, pp. 373-380.

RSI, 2002, ENVI version 3.5 User's Guide.

Smith, M.O. et al., 1994, A new approach to determining spectral abundances of mixtures in multispectral images. *Proc. IEEE Geosci. Remote Sens. Symp., IGARSS '94*.

Wohletz K.H. and M.F. Sheridan, 1983, Hydrovolcanic explosions II. Evolution of basaltic tuff rings and tuff cones. *Am. J. Sci.*, **283**, 385-413.